AD-A109 890 NORTHWESTERN UNIV EVANSTON IL DEPT OF MATERIALS SCIENCE F/G 11/6
THE PLASTIC ZONE AND RESIDUAL STRESS NEAR A NOTCH AND A FATIGUE--ETC(U)
DEC 81 W H SCHLOSBERG, J B COHEN N00014-80-C-0116
UNCLASSIFIED TR-5 NL

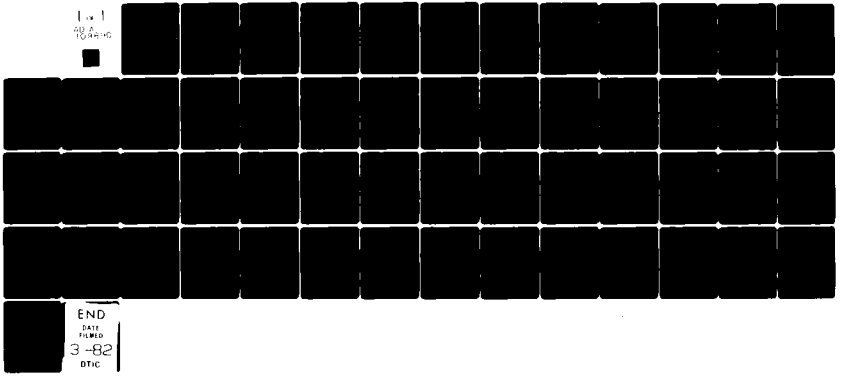

END
DATE FILMED
3-82
DTIC

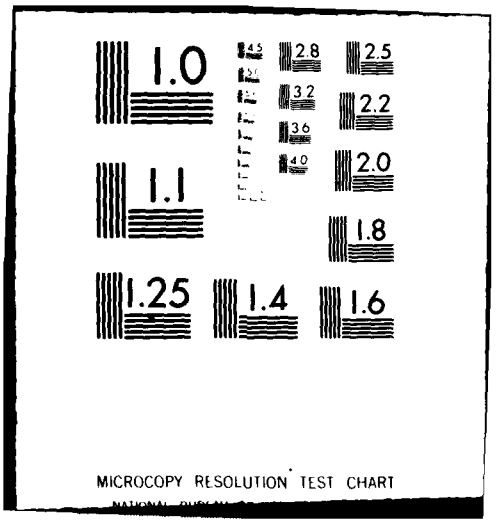
1.0
2.8
2.5
3.2
2.2
3.6
4.0
2.0
1.1
1.8
1.25
1.4
1.6
MICROCOPY RESOLUTION TEST CHART

LEVEL II

1

AD A109890

NORTHWESTERN UNIVERSITY

DEPARTMENT OF MATERIALS SCIENCE

Technical Report No. 5
December 16, 1981

Office of Naval Research
Contract N00014-80-C-0116

THE PLASTIC ZONE AND RESIDUAL STRESS NEAR A NOTCH AND A FATIGUE CRACK IN HSLA STEEL,

BY

W. H. Schlosberg and J. B. Cohen

EVANSTON, ILLINOIS

The Plastic Zone and Residual Stress Near a Notch and à Fatigue Crack in HSLA Steel[+]

by

W. H. Schlosberg[o] and J. B. Cohen[+]

ABSTRACT

The plastic zone and residual stress around a notch under load and with the load removed, and around a fatigue crack (at the same stress intensity factor as for the notch) have been examined, with automated X-ray techniques and a microbeam. There is good agreement between the measured plastic zone size and Hutchinson's theory for a work hardening material. Residual stresses exist well behind the tip, and vary with depth, so that measurements of crack closure on a surface may not be directly related to closure stress (which samples the bulk). Instabilities in the dislocation arrangement can be detected by comparing X-ray line broadening of bulk specimens under load, and with the load removed.

[o]W. H. Schlosberg, formerly research assistant, Dept. of Materials Science and Engineering, The Technological Institute, Northwestern University, Evanston, IL is now with Bendix Corp., Kansas City, Mo.
[+]J. B. Cohen, Fellow AIME, ASM, is Frank C. Engelhart Professor of Materials Science and Engineering, The Technological Institute, Northwestern University, Evanston, Illinois 60201

INTRODUCTION

It is well known that the stress singularity at a notch or crack tip produces local deformation, and that the associated plastic upset results in residual stresses in and around this region. The maximum extent of the stresses and deformation is not directly ahead or above the crack. While there have been many theoretical and expermental studies of these phenomena, no study (of which we are aware) has examined experimentally both the stresses and the plastic deformation simultaneously, in two dimensions, around a notch or crack. This is the purpose of this study.

Rice and Rosengren[1] and Hutchinson[2,3] have obtained theoretical solutions for the shape of the plastic zone, employing the Von Mises yield criterion, and allowing for work hardening. The former authors developed the solution for plane strain, with the shear stress, τ, expressed in terms of the yield shear stress, τ_y, and the shear strains, γ and γ_y : $\tau = \tau_y + \alpha(\gamma/\gamma_y)^n$. (1)

Here: $\tau = [\sigma_{ij}\,\sigma_{ij}/2]^{\frac{1}{2}}$, $\gamma = (2\epsilon_{ij}\epsilon_{ij})^{\frac{1}{2}}$, where τ and γ are stress and strain components, and repeated subscripts imply summation.
Hutchinson's solution is for plane stress, with flow described with the form:

$$\epsilon/\epsilon_y = \frac{\sigma}{\sigma_y} + \alpha\left(\frac{\sigma}{\sigma_y}\right)^N \quad . \tag{2}$$

In this case the work hardening exponent, N, is the inverse of n in Eq. 1. Both solutions assume that the stress singularity near the notch or crack can be approximated by the first term in an asymptotic series

expansion. Plastic zones calculated from these theories are illustrated in Fig. 1. For plane strain, the maximum extent of the zone moves closer to the crack plane as work hardening increases, assuming a "butterfly" shape. The zone size decreases with increasing work hardening exponent, for both plane stress and plane strain.

While these calculations are applicable to monotonic loading, their application to fatigue requires some caution, because both authors assume the stress is proportional to strain. Also, Rice[4] has indicated that there may be two plastic zones ahead of a fatigue crack, the outer one due to tensile loading, and the inner one due to reverse loading approximately one quarter the size of the outer one.

Experimental studies of the plastic zone are summarized in Table I. Except for the last entry,[21] the delineation of the zone has been rather arbitrary, (and other than the first entry) the agreement with theory poor. Fine et al.[21] have noted that agreement is good if the stress for zero hysteresis in incremental strain controlled fatigue is employed in the calculation, rather than the cyclic yield stress. (This stress is much less than the cyclic yield stress.) A number of experimentalists have noticed the "butterfly" shape of the zone, for example, refs. 6, 12, and 21.

It is well established that the residual stress immediately ahead of a fatigue crack and parallel to the aplied load is compressive, turns tensile at some distance, and then oscillates in sign, with decreasing magnitude. (There is no experimental study of a notch.) Indeed, it is also well established that the effect of an overload is

to increase this compressive stress in magnitude and extent, and to decrease crack velocity while the crack is in such a region.[22,23] Such stresses have been shown to aid crack closure.[22,24]

For the most part, the stresses have been measured only directly ahe.d of the crack, with X-rays. Rice's calculation[4] exhibits a region of constant compressive stress immediately ahead of the crack tip (in the reverse plastic zone), but this is due to the assumption of an ideally plastic material. Two finite element calculations[25,26] indicates the stress decreases in magnitude from the crack tip with a maximum value of approximately $2/3\,\sigma_y$. Some measurements[17,22,27,28] do indeed show the maximum stress at the tip, whereas others[8,17,29,30] report the maximum compression ahead of the tip. However, this might be due to uncertainty in locating the tip with respect to the X-ray beam. In all cases, the stresses are lower in magnitude than predicted by Rice. This difference has been attributed (for example in ref. 27) to the size of the X-ray beam, but this is definitely not the case in ref. 17.

Some of these authors report residual stresses slightly behind the crack tip, but usually attribute this, again, to the size of the X-ray beam. However, the beam was quite small in ref. 22, and furthermore, stresses were found well behind the tip; these are probably a result of the dislocations generated by the propagating crack.

The only two dimensional study of residual stresses (around the tip of a fatigue crack) is that of Allison[30]; however the uncertainty

in stress (±70 MPa) is quite high, only longitudinal stresses were measured, and the X-ray beam was much larger than the plastic zone.

EXPERIMENTAL PROCEDURES

Specimens

The major objective of this investigation is the mapping of the region around a crack tip. As the changes in the profile and position of an X-ray peak could be expected to occur in a region less than 1 mm in size, a very small X-ray beam is required. In a standard powder diffraction experiment with a beam typically 10,000 μm x 4,000 μm, a 25 μm grain size, and with the beam's penetration to this depth, 60,000 grains are irradiated. Special precautions are necessary to assure reproducibility of the diffraction profiles, if a beam the order of 100-200μm is to be employed. Therefore, a HSLA steel was chosen (Inland Steel Co. No. 328), because of its inherent fine grain size, 5 μm, so that the beam samples 5000 grains. (Tests on the reproducibility of the diffraction profile are reported below, in the section on X-ray measurements.) Its composition is given in Table II and it was obtained in the form of 3.4 mm thick sheets. Samples were prepared for: a) monotonic tensile testing (to examine the mechanical behavior and the effects of various levels of plastic deformation), b) to determine the X-ray elastic constants, c) with a center notch for fatigue testing. Strips 152 x 25 mm were sheared from these sheets, with the long dimension parallel to the original rolling direction. Mill scale was removed with a fly cutter, with a maximum cut of 0.5 mm. To minimize bending, specimens were given final dimensions with an end mill and a surface grinder (50 μm cuts under a liquid spray, with 13 μm

cuts in finishing passes). The geometries of the final specimens are shown in Fig. 2. When these specimens were machined, material was removed from one surface until the intensity of the 110 peak was a fixed value, the remainder of the material being removed from the opposite face. This was done to assure that the preferred orientation, which was present in all specimens, was the same at the surface to be exposed to the X-ray beam. Finishing was carried out with a chemical etch (200 parts 30% H_2O_2, 15 parts 48% HF), followed immediately by a wash in methyl alcohol and then in water. This etching was continued until the 110 $K\alpha_1$ - $K\alpha_2$ doublet resolution ceased to improve.

In experiments in which changes with depth were studied, a lacquer was applied, except in the area of interest, and the above chemical etch was employed. The thickness removed was measured with a micrometer, or from a calibration of thickness vs. time in the solution.

The center notch (Fig. 2b) was produced with an electric spark discharge, employing a pure copper electrode. Only specimens with narrow uniform notches within $\pm 3^{\circ}$ of the perpendicular to the tensile axis were employed. These samples were lightly etched again, after the notch was formed.

Mechanical Testing

Monotonic stress-strain curves were obtained on an Instron machine, employing a "clip-on" extensometer. Samples with various amounts of plastic deformation were also obtained in this manner, to compare their X-ray profiles to those near the plastic zone of a crack or notch.

To measure the X-ray elastic constants (see below), monotonic tests were conducted in the elastic range in situ, on a diffractometer, with a small device designed for this purpose;[31] this is essentially a set of grips in a channel, which can be separated by a thread with a fine pitch, coupled to a gear reducer. One revolution corresponds to 6.35 μm motion. A sample with a mounted extensometer was extended first on the Instron machine to obtain strain vs. load, and then, on the diffractometer, the extensometer reading was converted to stress.

Fatigue tests were carried on a servo-hydraulic instrument manufactured by MTS. The (pull-pull) tests were conducted at 10Hz, with an R ratio of 0.03-0.05. To minimize bending moments, the lower grip was placed in Wood's metal, which was melted during the mounting of the specimen. Crack extension was examined periodically with a 40x travelling microscope. X-ray measurements were obtained after the total length (crack-plus-notch) was approxmately half the width of the sample.

In order to compare the plastic zone sizes observed in this study with the various theories mentioned in the introduction, the yield strength (σ_y), ultimate tensile strength (σ_{UTS}), and work-hardening exponent (n), are needed for both monotonic and cyclic loading. To obtain n, the continuous portion of the monotonic tensile data was fitted to Eq. 1 with τ, γ replaced by σ, ε. The cyclic yield stress was defined from data[32] for another heat of the same steel, scaled by 13 pct. to compensate for a difference in the monotonic yield stress. The results are given in Table II.

X-ray Measurements

The X-ray source was a Rigaku rotating anode generator operated at 58kv, 10ma, with a fine focus filament (0.1 x 1 mm) and a Cu anode observed in point focus. With an intrinsic Ge detector and a single channel analyzer, Fe fluorescence could easily be separated from the incident CuK_{α} wavelength. A G.E. XRD-5 diffractometer was modified to fit this generator,[32] and a circular 100 μm divergence slit was employed for studies of the profile, with a standard 0.05° receiving slit. This divergence was increased to 400 μm and the receiving slit to 0.1° for stress measurements, because a weaker high-angle peak was involved.

At 45° 2θ (the position of the 110 reflection) the beam was 250 μm x 100 μm, (sampling some 5000 grains as mentioned above). The peak intensity was 5cps, with a background of 0.1 cps, and a (peak) width of 0.3° 2θ. A sample was oscillated ±1.5° to increase the sampling, and with this oscillation the peak intensity varied less than 15 pct. at different points on a sample.

To align some particular point on the specimen in the X-ray beam, the following procedure was developed. While observing under a low power microscope, a thin phosphor dot 100 μm in diameter was applied. The specimen was then placed on the diffractometer in a mount that could be displaced in x and y directions parallel to the face of the specimen, by amounts as small as 50 μm. These motions were employed until the maximum brightness from the dot (due to the X-rays) was obtained. (A series of divergence slits, 1 mm to 100 μm, were helpful at this stage.) A low power microscope on an adjustable bed attached

to the diffractometer was moved until its cross-hair was centered on this dot. The sample could then be moved to bring any desired location into the X-ray beam, by simply moving such a location to the cross-hair of the microscope.

X-ray intensities were accumulated by point counting, and processed with a minicomputer controlled diffractometer. The software was designed not only for data collection, but for on-line analysis, as will be described below. This software also included a routine for automatically aligning the sample over the diffractometer's axis. (The sample displacement was determined that minimized the differences in lattice parameter calculated from different peaks.) Computer interfacing included a 60 Hz signal from the rotating anode. If this signal vanished due to an inadvertent shut down as a result of an arc in the generator, all data were saved, and a simple restart procedure allowed measurements to continue after the generator was functioning again.

Analysis of the Data

A) Profiles

Fourier analysis of peak shape,[34] as modified by Delhez and Mittmeijer[35] was employed to obtain information on microstrains and mosaic size. The entire process of data collection and analysis was carried out on-line with a minicomputer control system based on a DEC PDP8-E computer. To minimize the well known effects of truncation in such an analysis, four precautions were followed: 1) at least ten values were obtained for the profile above 50 pct. of the maximum intensity, 2) this number of points was never less than 15 pct. of the

total number of points, 3) the region of the profile extended (on each side of the peak) at least four times the full width at half-maximum intensity, 4) analysis was carried out about the center of gravity of a peak, to minimize the sine coefficients.

All data were corrected for the Lorentz-polarization factor for step scanning, the variation of the structure factor, the Debye-Waller factor, and the dispersion-corrected scattering factor. Analyses were carried out on a $\sin\theta$ scale. The "hook" effect (the decrease in Fourier coefficients at very low harmonic number) was minimized following ref. 36, and the Fourier coefficients were corrected for instrumental broadening by Stokes' procedure.[37] The standard for this latter correction was one of the annealed specimens. The resulting Fourier cosine coefficient, A_n, of harmonic number n, can be witten:[35]

$$A_n = A_n^s \left(1 - 2\pi^2 n^2 a_3^2 \langle \epsilon_n^2 \rangle / d_{hk\ell}^2\right) \quad . \tag{3}$$

Here A_n^s is that portion of the coefficient due to mosaic size, D_{eff}, and a_3 is determined from the range of the peak:

$$\ell = \frac{2a_3}{\lambda} (\sin\theta_{max} - \sin\theta_{min}).$$

The value of $na_3 = L$ is the length of a column normal to the diffracting planes over which the beam is averaging the effects. Also, $\langle \epsilon_n^2 \rangle$ is the mean-square strain averaged over such a column, and $d_{hk\ell}$ is the spacing of the $(hk\ell)$ planes producing the reflection. The multiple order procedure for separating A_n^s and $\langle \epsilon_n^2 \rangle$ involves determining A_n at each n, for two or more orders of a reflection, ie. vs $\frac{1}{d^2}$. Then the average mosaic size normal to the $(hk\ell)$ diffracting planes (D_{eff}) is

obtained from:

$$\left(\frac{dA_n^s}{dn}\right)_{n\to 0} = -\frac{1}{D_{eff}} \quad . \tag{4}$$

Because of the low intensities of higher order peaks in this investigation with a microbeam (less than 1 cps for the 220 reflection, for example) it was decided to employ the single peak analysis developed by Mignot and Rondot.[38] For small n, $A_n^s = 1 - \frac{na_3}{D_{hk\ell}}$. Also, from ref. (5), $\langle \epsilon_n^2 \rangle = \frac{G^2}{na_3}$, where G is a constant. Substituting these relationships into Eq. 3, Mignot and Rondot showed that:

$$A_n = 1 - n\left\{\frac{a_3}{D_{eff}} + 2\pi^2 a_3 G^2/d_{hk\ell}^2\right\} + n^2\left\{\frac{2\pi^2 a_3^2 G^2}{d_{hk\ell} D_{eff}}\right\} \tag{5}$$

$$= \alpha + n\beta + n^2\gamma \quad . \tag{6}$$

By algebraic manipulation of Eqn. (5):

$$D_{eff} = 2a_3/\left[-\beta + (\beta^2 - 4\gamma)^{\frac{1}{2}}\right] \tag{7a}$$

$$G^2 = d_{hk\ell}^2\left\{-\beta - (\beta^2 - 4\gamma)^{\frac{1}{2}}\right\}/\, 4\pi^2 a_3 \tag{7b}$$

A least squares solution of Eqn. 6 (for α, β, γ) was obtained with various combinations of low-order A_n (but excluding A_o). All solutions involving the first 4–10 coefficients were obtained. Those with negative were rejected. The remaining solutions were ranked (by the software) by considering that: 1) α should be unity, 2) β should be the initial slope of A_n vs n, 3) the unbiased residual should be a

minimum.

Both the single and multiple-peak methods and all corrections have been fully implemented in the software. Errors in the resultant values of the microstrain and particle size were obtained from the variances and co-variances of the Fourier coefficients, which depend on the number of counts collected across a peak. The equations for these are given in the Appendix. The software was written so that counting over a peak was repeated until the root mean relative variance of the first few Fourier coefficients (which are the ones that are important in determining D_{eff} and G) was an operator-specified value, σ_1:

$$\sigma_1 = \left\{ \sum_{j=1}^{r} \frac{\sigma^2(A_j)}{A_j^2} \right\}^{\frac{1}{2}} \Big/ n \, . \tag{8}$$

Actually, the square root of the sum of the squares of σ_1 for the reference and broadened profiles was employed.

Such automation does more than minimize manual operations. It also minimizes the time to obtain a reasonable precision. In the past, this type of analysis has been carried out by obtaining the data, plotting and smoothing it, subtracting background by hand, and punching cards for a program for a large computer to perform corrections and/or the Fourier analysis. In general, no error analysis is possible and data are usually obtained for times considerably longer than needed. Some idea of the error can be obtained by repeating measurements and analysis, but this is rarely done. This older procedure is still necessary for very broad, weak peaks with low peak-to-background ratios, but the new procedures described here are applicable in most

situations. It is possible to obtain the data and a complete 2-peak analysis with normal beams in 3 hours.

Comparisons were made of the single and multiple peak procedures, employing data obtained in several past studies in our group. In general, if the peak-to-background ratio is large, and the mosaic size is 200-500 Å , the single peak method is viable; otherwise it is not. In particular, values for $\langle \epsilon_n^2 \rangle$ are very poorly determined outside this range, although the particle size is satisfactory. Fortunately, our studies fell within these boundaries. Some of the comparisons we have made are given in Table III.

B) Analysis for Residual Stress

The 222 reflection was employed, which occurs at 136° 2θ with the CuK_α radiation employed in this research. The maximum intensity was 2 cps (with a background of 0.1 cps). Because this peak occurs at angles somewhat lower than those commonly employed for stress measurements from steel with Co or Cr radiation (and which are too low in intensity for this study) the peak position is more sensitive than usual to sample position, often the major source of error in stress measurements. Therefore, particular care was taken to be sure that the surface of a specimen was within 25 μm of the center of the diffractometer. This peak does have an advantage though, in that it is unaffected by preferred orientation and the attendant elastic anisotropy [44] this can cause strong oscillations in d spacing vs $\sin^2\psi$ (where ψ is the tilt of the specimen from the parafocussing position); it is from the slope of such a plot that the stress is calculated.

Four ψ tilts were employed initially, from 0° to 45°, but this was reduced to three when it was found that "d" vs $\sin^2\psi$ was indeed quite linear (correlation coefficient > 0.93). At each tilt, the same 3° oscillation employed in studies of the profile was also used. A multi-point parabola was fit to the top 15 pct. of the peak, following ref. (44). The entire process was automated, as described in this reference. Statistical counting errors and geometric errors (also see ref. [44]) were evaluated in the software and were typically a total of ± 20MPa, which was confirmed by repeated measurements.

To obtain the appropriate X-ray elastic constants, a tensile specimen (Fig. 2) was mounted in the small tensile jig described above. The stress was kept below 2/3 σ_y, to minimize plastic deformation at the surface. The slope of "d" vs. $\sin^2\psi$ was obtained for various stresses. Now:

$$A = \left[\frac{\partial(\Delta d)}{\partial \sin^2\psi}\right] \equiv d_o \frac{S_2}{2}\sigma , \qquad (9)$$

where $\frac{S_2}{2}$ is the effective elastic constant. From A vs σ_1, $\frac{S_2}{2}$ was obtained, so that Eqn. 9 could then be employed for specimens with unknown stresses. The value of $\frac{S_2}{2}$ was 5.08(1.26) x 10^{-6} MPa.$^{-1}$ With the bulk elastic constants in ref. 46, an average value of this constant for constant strain and constant stress[47] gave 4.98 x 10^{-6} MPa.$^{-1}$ The experimental value was employed for all stresses reported here.

RESULTS

A Working Definition of the Plastic Zone

The results of the Fourier analysis of peak shape after tensile elongation are presented in Table IV. Distinct changes in mosaic size and microstrain occur at 0.1 pct. permanent offset, after which, and until necking begins, these quantities are approximately constant. It has been shown[48,49] that the mosaic size and microstrain are related to the dislocation spacing, and therefore to the dislocation density, ρ. From the mosaic size "ρ_D" can be calculated:

$$\rho_D = \frac{1}{D_{eff}^2} \quad , \tag{10}$$

and from the microstrain, "ρ_S":

$$\rho_s = 12 \langle \epsilon_{50\text{Å}}^2 \rangle / b^2 \quad , \tag{11}$$

where b is the Burger's vector.

The limit of this analysis in this study, due to instrumental broadening of the 110 peak, corresponds to a mosaic size of 3500Å. Therefore, Table IV implies a change in dislocation density at 0.1 pct. offset from $\sim 8 \times 10^{12}$ m^{-2} to 1.6×10^{14} m^{-2}. Accordingly, we have chosen $D_{eff} = 2500$Å ($\rho = 1.6 \times 10^{13}$ m^{-2}) to delineate the plastic zone. This region is shaded in several of the subsequent figures. It is worth repeating that the size of the X-ray beam on a sample was always considerably smaller than this zone.

Residual Stresses

One sample 2 mm thick, with a 5.7 mm notch and a root radius of 64 μm, was stressed at 308 MPa ($\frac{\sigma}{\sigma_y} = 0.52$) so that K_I (calculated

following Paris and Sih,[50] including the correction for the finite width of the sample) was 30.2 MPa $m^{1/2}$. The sample was unloaded, loaded again, unloaded and loaded once more. It requires about 10^3 cycles at this load to initiate a crack from a notch of this kind, so this procedure produces a plastic zone ahead of the notch, without propagation. The longitudinal and transverse stresses measuring under load are shown in Fig. 3, after removing the load in Fig. 4, and , after etching to remove one quarter of the thickness to the center of the specimen, Fig. 5. [This etching was carried out only in the vicinity of the notch, by masking, as indicated in the procedures. Therefore no appreciable relief of stress due to this removal of material was expected, and no corrections were applied to the data.] In Fig. 3, it can be seen that about 0.8 mm above the notch, the measured longitudinal stress under load was (within experimental error) the applied stress. Note also that after removing the load the compressive stress near the notch tip is large at the surface but decreases considerably with depth.

A second specimen, 2.05 mm thick, with a notch 4.8 mm long and a root radius of 29 μm was subject to fatigue at a maximum stress of 208 MPa with a stress range of 200 MPa, for 70,000 cycles, after which a crack had grown 3.5 mm from both ends of the notch. The value of K_I was 17.7 MPa $m^{1/2}$ at the beginning of the test, and 31.3 MPa $m^{1/2}$ at the end. This latter value is quite close to the value employed above for the notched specimen. The measured residual stresses are given in Fig. 6. The maximum value is less than the value of 2/3 σ_y predicted in ref. 25.

Of particular interest is the presence of residual stress behind both the notch and fatigue crack, and the fact that the stresses extend well beyond the plastic zone.

Analysis of Peak Shape

Typical errors in particle sizes (which were the order of 1200-3000Å) and microstrains were 25 pct. The Figs. 7,8,9 exhibit dislocation densities calculated at various locations for the sample with a notch, and for the fatigued sample. The value shown is the square root of the product of Eq. 10 and 11, that is, the average of the two values. Due to the errors in D and the uncertainty in these values is 50 pct. The density was usually smaller by a factor of two to three when calculated from the mosaic size, implying that the dislocations are clustered. It is particularly interesting that the density immediately ahead of the notch (in the statically loaded specimen) increases when the load is removed. This result implies that dislocations move away from tangles and walls on unloading. The unstable nature of dislocation arrays in the early stages of fatigue is well known.[51] Also, the density just ahead of the fatigue crack is higher than ahead of the more blunt notch, and there is more clustering of dislocations ahead of the fatigue crack; the opposite is true above the crack. These patterns are in general agreement with Mugrabi's TEM studies.[51] The dislocation densities just ahead of the fatigue crack found in this study are of the same order of magnitude as those found by Yokobori et al.[17,18] with the Hirsch microbeam technique applied to a low carbon steel. However, they reported a decrease of two orders of magnitude in density 200 μm ahead of the crack. We see much less variation.

Yokobori and Sato[19] examined the density of dislocations near a crack (in a low carbon steel) at various positions below the surface, and found little change up to 400 μm from the surface. On the other hand, Pangborn et al.[52] employing a smooth aluminum fatigue specimen, reported a decrease by a factor of three 100 μm below the surface (followed by an increase again at greater depths). We made measurements of the peak breadth at four positions near the fatigue crack at 50, 130, 190 and 250 μm below the surface, and there was no noticeable change in broadening. It seems clear that near a fatigue crack, the dislocation density does not vary appreciably with thickness. This is actually to be expected from Pangborn's results, which indicate that failure occurs when the dislocation density in the interior rises to that near the surface. Such a situation would be likely in the plastic zone just ahead of a crack or notch.

DISCUSSION

The specimen thickness used in this study (2 mm), is much less than required for plane strain conditions to dominate; from ref. 6, this thickness would be approximately 10 mm for the steel used here. For this reason, and also because the X-rays sample only the near surface regions, measurements on the face of the samples should resemble what is expected for plane stress. For the sample with a notch, the fact that the residual stress pattern extends much further normal to the notch than ahead of it suggests that plastic upset inside the specimen, where conditions for plane strain exist, are important even near the surface.

The "butterfly" shape ahead of the notch or crack is clear in our results for σ_{yy}, but not in the plastic zone itself (defined here as equivalent to 0.1 pct. plastic offset in tension). The regions of residual stress need not have suffered plastic deformation but could develop due to upset in the smaller plastic zone. The stresses would of course affect stress-strain hysteresis, and this may be the reason that a very low stress is required in ref. 21 to calculate a "plastic zone" of the size the authors measured; the zone delineated by stress hysteresis may actually be the region of appreciable residual stress. With the data obtained in this study on yield stress and plastic zone size, a direct comparison of calculated and measured plastic zone sizes is possible. This comparison is shown in Table V, where it can be seen that the agreement is quite good for the expected conditions of plane stress, especially for the specimen with a fatigue crack.

According to Rice[4] and Matsuoka and Tanaka[53] the plastic zone size is $\sim$ 1.6 times the position ahead of the crack where the stress reverses sign. This value is 1000 μm, only 30 pct. bigger than the measured value, so this appears to be a viable method for estimating the size. A reverse plastic zone of 250 μm would also be expected in this case. Although the size of the X-ray beam employed in our experiments was almost half this value, we could not detect any unusual broadening or stresses very close to the crack that would suggest such a region.

Because crack closure is affected by residual stresses, it is of particular interest that the stresses are much lower inside the

specimen than at the surface. There are, of course, other factors that can lead to different closure at the surfce and in the bulk, such as oxidation,[54] and the differences in the stress state;[55] all three reasons complicate the relationship between crack closure measured optically and closure stress.

SUMMARY

1) A quantitative X-ray study of the substructure and residual stresses has been made inside and outside the plastic zone associated with a notch and with a fatigue crack. A deformation corresponding to little as 0.1 pct. plastic offset in tension could be detected.

2) The instability of dislocation arrangements in such regions is clearly indicated by changes in X-ray peak shape under load, vs load removed.

3) There is good agreement between Hutchinson's theory for plane stress and experiments on the size and shape of the plastic zone, for both a notch and a fatigue crack.

4) There are appreciable residual stresses behind a notch or crack, as well as above and ahead of this region.

5) The residual stress distribution can vary appreciably with depth. As a result of this (and other variations between the surface and the interior) optical measurements of crack closure at a surface may not be simply related to the stress for crack closure.

ACKNOWLEDGEMENTS

This research was supported by ONR under contract No. N00014-78-0079. The X-ray studies were performed in Northwestern University's X-ray diffraction facility supported in part by the NSF-MRL program under grant No. DMR-MRL - 76-80847. This research represents portions of a Ph.D. thesis submitted by one of the authors (W.H.S.) in partial fulfillment of the requirements for the Ph.D. degree at Northwestern University. He acknowledges Northwestern University's Murphy fund and International Nickel Co. for fellowships. Both authors thank Mr. J. Hahn for his assistance and design in constructing the apparatus, and Mr. R. Karhuse for guidance with the computer programming. Profs. M. E. Fine (Northwestern University) and Prof. H. Marcus (University of Texas-Austin) kindly provided critical comments on the manuscript.

APPENDIX

Errors in the Warren-Averbach Fourier Analysis of Peak Shape Due to Counting Statistics, and Automation of the Analysis.

A. Multiple Peaks, Eq. 1

It is rare to have more than two orders of a given reflection within the observable 2θ range, so we deal with this case here. This is readily extended, if more peaks are available. The peaks are given subscripts 1, 2.

From Eq. 3, A_n is linear vs $1/d_{2hk\ell}$. Therefore, by manipulating this equation for each of two peaks (subscripts 1 and 2), to yield the slope and intercept of A_n vs 1/d, the variance (σ^2) can be written as:

$$\sigma^2(\text{intercept}) = \{(\sigma(A_{n1})/d_2^2)^2 + (\sigma(A_{n2})/d_1^2)^2\} \qquad \text{(A-1a)}$$

$$/\{1/d_1^2 - 1/d_2^2\}^2,$$

and:

$$\sigma^2(\text{slope}) = \{\sigma^2(A_{n1}) + \sigma^2(A_{n2})\}/\{1/d_1^2 - 1/d_2^2\}. \qquad \text{(A-1b)}$$

The equation for (A_n) is discussed below, section C).

From ref. 38:

$$\sigma^2\langle\epsilon_n^2\rangle^{\frac{1}{2}} = (\partial\langle\epsilon_n^2\rangle^{\frac{1}{2}}/\partial \text{ slope})^2\,\sigma^2(\text{slope}) + (\partial\langle\epsilon_n^2\rangle^{\frac{1}{2}}/\partial \text{ intercept})^2\sigma^2(\text{intercept}), \qquad \text{(A-2)}$$

and hence:

$$\sigma^2(A_n^s) = \sigma^2(\text{intercept}), \qquad \text{(A-3a)}$$

$$\sigma^2(\langle\epsilon_n^2\rangle^{\frac{1}{2}}) = \tfrac{1}{4}\langle\epsilon_n^2\rangle\{\sigma^2(\text{slope})/\text{slope}^2 + \sigma^2(\text{intercept})/\text{intercept}^2\}. \qquad \text{(A-3b)}$$

The error for the particle size (see Eqn. 3) can then be obtained from the error in the slope of a (weighted linear least-squares) fit to A_n^s vs n, for small n.

B. Single Peak, Eq. 3

At least four Fourier coefficients of low order (low n or L) are employed to solve this equation by least-squares, as for example, in Ch. 4 of ref. 39. However, the first coefficient, A_0, cannot be employed; its value is unity by definition, and therefore its variance and co-variance with other coefficients is null. Again, following ref. 38, and keep in mind that the least squares analysis of Eq. 6 yields $\sigma^2(\beta)$, $\sigma^2(\gamma)$:

$$\sigma^2(Q) = \left(\frac{\partial Q}{\partial \beta}\right)^2 \sigma^2(\beta) + 2\,\frac{\partial Q}{\partial \beta}\,\frac{\partial Q}{\partial \gamma}\,\mathrm{COV}(\beta,\gamma) + \left(\frac{\partial Q}{\partial \gamma}\right)^2 \sigma^2(\gamma), \qquad \text{(A-4)}$$

Here "COV" means covariance.

we define $Q = -\beta + (\beta^2-4\gamma)^{\frac{1}{2}}$ for the calculation of $\sigma(D_{eff})$,

and $Q = -\beta - (\beta^2-4\gamma)^{\frac{1}{2}}$ for $\sigma(G^2)$, since from Eqs. 5,6:

$$D_{eff} = 2a_3/\{-\beta + (\beta^2 - 4\gamma)^{\frac{1}{2}}\}, \qquad \text{(A-5a)}$$

$$G^2 = d^2\{-\beta-(\beta^2-4\gamma)^{\frac{1}{2}}\}/4\pi^2\, a_3. \qquad \text{(A-5b)}$$

Therefore, with these definitions and Root $\equiv (\beta^2 - 4\gamma)^{\frac{1}{2}}$ it can be shown that:

$$\sigma(D_{eff}) = \{(-1 + \beta/\mathrm{ROOT})^2\,\sigma^2(\beta) + 4(-1/\mathrm{ROOT})^2\,\sigma^2(\gamma) + 4(-1+\beta/\mathrm{ROOT})(-1/\mathrm{ROOT})\mathrm{COV}(\beta,\gamma)\}^{\frac{1}{2}} D_{eff}/2a_3 \qquad \text{(A-6a)}$$

and:

$$\sigma(G^2) = \{(-1 -\beta/\mathrm{ROOT})^2\sigma^2(\beta) + 4(1/\mathrm{ROOT})^2\sigma^2(\gamma) + 4(-1 -\beta/\mathrm{ROOT})(1/\mathrm{ROOT})\mathrm{COV}(\beta,\gamma)\}^{\frac{1}{2}} \cdot d^2/4\pi^2\, a_3. \qquad \text{(A-6b)}$$

The least squares analysis for α , β , γ in Eq. 6 require a knowledge of the variance of Fourier coefficients A_n^s (see ref. 16) as does the error analysis for two or more peaks in part A. Therefore we turn now to this variance.

C. Variance of the Fourier Coefficients

Wilson[40-42] has derived equations for the variances of the Fourier cosine coefficients ($\sigma^2(A_n)$) and sine coefficients ($\sigma^2(B_n)$) of a Bragg peak, as well as their co-variances. He ignored certain small terms, which we include here, as the calculations are to be carried out on a computer. For details of the derivations, the reader is referred to Wilson's papers and ref. 32.

Assuming the background is linear:

$$A_o = \frac{\sum_{j=-r}^{r} [I_j - (g + (G_R - G_L)\, j/R)] \cos(2\pi n j/R)}{\sum_{j=-r}^{r} [I_j - (g + (G_R - G_L)\, j/R)]} , \qquad \text{(A-7)}$$

where: I_j = measured intensity at the jth point,

g = average background,

G_R and G_L = background intensitiesat the right (r) and left (-r) end points, respectively,

R = total number of points, $2r+1$,

A_o = total area under the curve.

By expanding the numerator and denominator and simplifying:

$$A_n = \frac{\sum_j [I_j - g] \cos(2\pi n j/R)}{\sum_j [I_j - g]} . \qquad \text{(A-8)}$$

Following standard methods of error propogation [38] the variance

of A_n may be expressed as:

$$\sigma^2(A_n) = \sum_k \left(\frac{\partial A_n}{\partial I_k}\right)^2 \sigma^2(I_k). \qquad \text{(A-9)}$$

For fixed-time measurements:[40]

$$\sigma^2(I_k) = I_k/T, \qquad \text{(A-10)}$$

where T is the measurement time per point.

From Eq. A-9 and A-10, with L_o the background corrected integrated intensity:

$$\sigma^2(A_n) = \frac{1}{TL_o^2}\{\tfrac{1}{2}\Sigma I_k + \tfrac{1}{2}\Sigma[I_k - g]\cos(4\pi nk/R) + g[\cos(4\pi nk/R) - 2A_n\Sigma[I_k - g]\cos(2\pi nk/R) - 2A_n g\Sigma\cos(2\pi nk/R) + A_n^2\Sigma I_k\}. \qquad \text{(A-11)}$$

The individual terms in the previous expression may be rewritten as:

$$\begin{aligned} &\text{first:} && (L_o + Rg)/2, \\ &\text{second:} && L_o A_{2n}/2, \\ &\text{fourth:} && -2A_n^2 L_o, \\ &\text{sixth:} && A_n(L_o + Rg). \end{aligned} \qquad \text{(A-12)}$$

Combining these terms allows equation (A-11) to be rewritten:

$$\sigma^2(A_n) = \frac{1}{TL_o^2}\{A_n^2(Rg - L_o) + [A_{2n}L_o]/2 + [L_o + Rg]/2 + g[\tfrac{1}{2}\Sigma\cos(4\pi nk/R) - 2A_n\Sigma\cos(2\pi nk/R)]\}. \qquad \text{(A-13)}$$

A similar analysis starting with the definition of the covariance between the nth and mth Fourier coefficients:

$$\mathrm{COV}(A_n, A_m) = \sum_k \left(\frac{\partial A_n}{\partial I_k}\,\frac{\partial A_m}{\partial I_k}\right)\sigma^2(I_k), \qquad \text{(A-14a)}$$

gives the following result:

$$\mathrm{COV}(A_n, A_m) = \frac{1}{TL_o^2}\{A_n A_m(Rg - L_o) + [A_{n+m}L_o]/2$$

$$+ [A_{n-m}L_o]/2 + g[\tfrac{1}{2}\Sigma\cos(2\pi[n+m]k/R)$$

$$+ \tfrac{1}{2}\Sigma\cos(2\pi[n-m]k/R) \cdot$$

$$- A_m\Sigma\cos(2\pi mk/R) - A_n\Sigma\cos(2\pi nk/R)] \quad . \qquad \text{(A-14b)}$$

In a completely analogous manner the variance of the Fourier sine coefficients, B_n, is obtained starting with:

$$B_n = \frac{\Sigma_j[I_j - (g + (G_R - G_L)j/R)]\sin(2\pi nj/R)}{\Sigma_j[I_j - (g + (G_R - G_L)j/R)]} \quad , \qquad \text{(A-15a)}$$

and:

$$\sigma^2(B_n) = \Sigma_k\left(\frac{\partial B_n}{\partial I_k}\right)^2 \sigma^2(I) \quad , \qquad \text{(A-15b)}$$

giving:

$$\sigma^2(B_n) = \frac{1}{TL_o^2}\,[B_n^2(Rg - L_o) - [A_{2n}L_o]/2 + [L_o + Rg]/2$$

$$-[\tfrac{1}{2}g\Sigma\cos(4\pi nk/R)$$

$$+2B_n(G_R - G_L)/R\Sigma k\sin(2\pi nk/R)]] \quad . \qquad \text{(A-15c)}$$

Equation (A-12) can be used as the criterion for determining the time for data collection, as well as for the analysis of errors. Given that the initial time for data collection which is specified by the user, T, is long enough to measure a statistically significant number of counts, the total time of data collection can be predicted from the expression:

$$\frac{\sigma_1^2(A)}{\sigma_D^2(A)} = \frac{T}{T_1} \qquad \text{(A-16)}$$

where $\sigma_1^2(A)$ is the variance calculated for a measurement for time T_1, and $\sigma_D^2(A)$ is the desired variance; T is the required counting time. In practice the Fourier coefficients will vary slightly as a function of the counting time and, therefore, the predicted total time may prove insufficient. Since the process is iterative, the sequence of steps

is:

1) measure quickly,

2) calculate Fourier coefficients and variances,

3) calculate additional counting time.

This sequence may have to be repeated a third or even a fourth time.

The method of specifying the desired variance should take into account that a number of Fourier coefficients are needed to determine the particle size and root-mean-square strain. One way to accomplish this is to define the allowable error as the root-mean relative variance:

$$\sigma_D(A) = \left\{ \sum_{j=1}^{n} \frac{\sigma^2(A_j)}{A_j^2} \right\}^{\frac{1}{2}} / n \quad . \tag{A-17}$$

However, since only the initial Fourier coefficients are used to determine the strain and particle size, σ_D can be limited to include coefficients up to an arbitrary maximum. In our case coefficients up to a column length, $L = na_3$, of 200 Å with an arbitrary maximum of $n = 5$ were used. Since A_0 is unity by definition, it is not included in this calculation. If Fourier coefficients are known for both the reference and the broadened profile, the square root of the sum of the two root-mean relative variances is a suitable estimate of the root-mean relative variance of the Stokes corrected profile. This was used in this study to determine the counting times.

D. Features of the Program

1. An initial dialogue with the operator requests pertinent information, such as the appropriate equation for the Lorentz-

polarization factor, absorption coefficients, scattering factors, oscillation range, 2θ limits, deadtime, wavelength, preset time or count, 2θ range of peak and step interval (which may be different in different regions of a peak), and percent error desired in the Fourier coefficients. Input information which varies with 2θ is fit with a cubic spline function.

2. As a peak is analyzed, various facets of the analysis are printed and plotted, to allow the operator to change items, or, for example, to choose a different set of A_n in the one peak analysis. The output includes the particle size and strain and the associated errors.

For further details, see ref. 32. A program listing as well as a user's manual are available from the second author.

REFERENCES

1. J. R. Rice and G. F. Rosengren: J. Mech.Phys. Sol., 1968, Vol. 16, pp. 1-12.

2. J. W. Hutchinson: J. Mech. Phys. Sol., 1968, Vol. 16, pp. 13-31.

3. J. W. Hutchinson: J. Mech.Phys. Sol., 1968, Vol. 16, pp. 337-347.

4. J. R.Rice: "Mechanics of Crack Tip Deformation and Extension by Fatigue", ASTM Spec. Tech. Pub. 415, 1967, pp. 247-311.

5. G. T. Hahn and A.R. Rosenfield: Acta Met., 1965, Vol. 13, pp. 293-306.

6. G. T. Hahn, R. G. Hoagland and A. R. Rosenfield: Met. Trans., 1972, Vol. 3, pp. 1189-1202.

7. D. S. Dugdale: J. Mech. Phys. Sol., 1960, Vol. 8, pp. 100-104.

8. S. Taira and K. Tanaka: Eng. Frac. Mech., 1972, Vol. 4, pp. 925-938.

9. Y. Iino: Eng. Frac. Mech., 1975, Vol. 7, pp. 205-218.

10. H. W. Liu and N. Iino: 2nd Int'l Conf. on Fracture (P. L. Pratt, ed.) Chapman Hall, London, 1969, pp. 812-824.

11. G. Marci, P. F. Packman and J. W. Jones: 2nd Int'l Conf. on Mech. Behavior of Mat'ls, ASM, Metals Park, Ohio, 1976, pp. 583-589.

12. P. S. Theocaris and E. Marketos: J. Mech. Phys. Sol., 1963, Vol. 11, pp. 411-428.

13. C. Bathias and R. M. Pelloux: Met. Trans., 1973, Vol. 4, pp. 1265-1273.

14. A. G. Pineau and R. M. Pelloux: Met. Trans., 1974, Vol. 5, pp. 1103-1112.

15. D. L. Davidson and J. Lankford: Trans. ASME, 1976, Vol. 98H, pp. 24-29.

16. J. Lankford and D. L. Davidson: Trans. ASME, 1976, Vol. 98H, pp. 17-23.

17. T. Yokobori, K. Tachikawa and A. Kamei: Rep. Res. Inst. Strength and Frac. of Mat., Tohoku Univ., 1970, Vol. 6, pp. 1-17.

18. T. Yokobori, K. Sato and Y. Yamaguchi: Rep. Res. Inst. Strength and Frac. of Mat., Tohoku Univ., 1970, Vol. 6, pp. 49-67.

19. T. Yokoburi and K. Sato: Rep. Res. Inst. Strength and Frac. of Mat., Tohoku Univ., 1972, Vol. 8, pp. 43-53.

20. T. Yokoburi, K. Sato and H. Yaguchi: Rep. Res. Inst. Strength and Frac. of Mat., 1973, Tohoku Univ., Vol. 9, pp. 1-10.

21. P.K. Liaw, M. E. Fine and D. L. Davidson: Fatigue of Eng. Mat. and Structures, 1980, Vol. 3, pp. 59-74.

22. K. Honda, T. Konaga and N. Tom: Non destructive Testing (Japan), 1979, Vol. 28, pp. 243-249.

23. D. R. Holloway: Final Report AFFDL-TR-79-3006, 1979, Air Force Flight Dynamics Laboratory, Wright-Patterson AFB, Ohio.

24. W. Elber: "The Significance of Fatigue Crack Closure," ASTM Spec. Tech. Pub. 486, 1971, pp. 230-242.

25. K. Ogura and K. Ohji: Eng. Frac. Mech., 1977, Vol. 9, pp. 471-480.

26. L. Kunt: Fatigue of Eng. Mat. & Str., 1979, Vol. 2, pp. 279-287.

27. G. Hellwig and E. Macherauch: Z. Metallk., 1974, Vol. 65, pp. 496-500.

28. E. Macherauch: Harterei-Techn. Mitt., 1976, Vol. 31, pp. 43-47.

29. Society of Automotive Engineers, Minutes of Fatigue Division, Annl. Meeting SAE Fatigue Design and Evaluation Committee, 1975.

30. J. E. Allison: AFFDL TLR 78-24, 1978, Air Force Flight Dynamics Laboratory, 1978, Wright Patterson AFB, Ohio.

31. R. H. Marion and J. B. Cohen: Adv. in X-ray Anal., 1977, Vol. 20, pp. 355-367.

32. J. J. Perout: M.S. thesis, 1976, Northwestern University, Evanston, IL.

33. W. H. Schlosberg, Ph.D. thesis 1979, Northwestern University, Evanston, IL. 60201.

34. B. E. Warren: Progress in Met. Phys., 1959, Vol. 8, pp. 147-202.

35. R. Delhez and E. J. Mittemeijer: J. Appl. Cryst., 1976, Vol. 9, pp. 233-234.

36. R. L. Rothman and J. B. Cohen: J. Appl. Phys., 1971, Vol. 42, pp. 971-979.

37. A. R. Stokes: Proc. Phys. Soc. London, 1948, Vol. 61, pp. 382-391.

38. J. Mignot and D. Rondot: Acta. Met., 1975, Vol. 23, pp. 1321-1324.

39. Y. Beers: "Introduction to the Theory of Errors," 1957, Addison-Wesley Publ. Co., Reading, Mass.

40. W. C. Hamilton: "Statistics in Physical Sciences", 1964, Ronald Press, New York, N. Y., pp. 124-145.

41. A. J. C. Wilson: Acta. Cryst., 1967, Vol. 23, pp. 888-898.

42. A. J. C. Wilson: Acta. Cryst., 1968, Vol. A24, P. 478.

43. A. J. C. Wilson: Acta. Cryst., 1969, Vol. A25, pp. 584-585.

44. H. Dölle: J. Appl. Cryst., 1979, Vol. 12, pp. 489-501.

45. M. R. James and J. B. Cohen: Adv. in X-ray Anal., 1977, Vol. 20, pp. 291-308.

46. W. J. M. Tegart: "Elements of Mechanical Metallurgy", 1966, McMillan, New York, P. 89.

47. H. Neerfield: M. H. KWI Eisenforsch., 1942, Vol. 24, P. 61.

48. D. E. Mikkola and J. B. Cohen: Acta. Met., 1966, Vol. 14, pp. 105-122.

49. D. C. Brillhart, R. J. DeAngelis, A. G. Preban, J. B. Cohen and P. Gordon: Met. Trans., 1967, Vol. 239, pp. 836-843.

50. P. C. Paris and G. C. Sih: ASTM Spec. Tech. Pub. 381, 1964, pp. 30-81.

51. H. Mughrabi: Phil. Mag., 1971, Vol. 23, pp. 931-947.

52. R. N. Pangborn, S. Weissmann and I. R. Kramer: Scripta Met., 1978, Vol. 12, pp. 129-131.

53. S. Matsuoka and K. Tanaku: Eng. Frac. Mech., 1976, Vol. 8, pp. 507-523.

54. D. S. Mahulikar and H. L. Marcus: Fatigue of Eng. Materials and Structures, 1981, Vol. 3, pp. 257-264.

55. D. S. Mahulikar, W. P. Slagle and H. L. Marcus, Scripta Metall., 1979, Vol. 13, pp. 867-870.

TABLE I

Prior Experimental Studies of Plastic Zones

Technique	Measured/Calculated Zone Size	Relative Load	Comments
Etch pit density[5,6]	0.7-1	$\frac{\sigma}{A} = 0.7\text{-}0.5$ $\left(\frac{\Delta K}{\sigma_y}\right)^2 = 2\text{-}4$ mm	Monotonic and Fatigue Loading. Only a limited number of materials can be examined; zones for plane strain and stress obtained, depending on specimen thickness.
Slip band density[7,8]	Much larger than theory		
Recrystallized grain size[9]	———	———	Size decreased, increased then decreased again with uniaxial tensile strain, so difficult to interpret.
'Moire' patterns[10,11]	———	———	Difficult to employ for fatigue, as smooth surfaces needed.
Birefringent plastic coatings[12]	———	———	Can't exceed elastic region of film. Difficult in fatigue to maintain bonding and must assume no effect on yielding. Zone really defined by theory.
Microhardness[13,14]	0.5	$\left(\frac{\Delta K}{\sigma_y}\right)^2 = 0.4\text{-}2.8$mm	Inner cyclic zone seen in fatigue. Marked cyclic hardening or softening required.
SEM-channelling[15,16]	3-5	$\left(\frac{\Delta K}{\sigma_y}\right)^2 = 1.5$ mm	Zone defined as region where channelling was same as 3% elongation. (Using a smaller strain makes comparison worse.)
X-ray microbeam[8,17-20]	<0.3 to > 2	various $\frac{\sigma}{\sigma_y} \sim 0.6$	Transition from spotty to continuous diffraction rings used as definition, and compared to slip pattern. X-ray zone 1/7 to 1.5 x larger. When dislocation density = bulk value is definition, $r_p \propto \Delta K^2$
Strain gauges[21]	1/7	$\left(\frac{\Delta K}{\sigma_y}\right)^2 \sim 50$ mm (σ_y = 0.2% offset cyclic yield)	Hysteresis loops mapped around crack and loop area extrapolated to zero.

TABLE II

Composition of Inland Steel Co. HSLA 328 Alloy and Mechanical Properties.

ELEMENT	Wt. %
C	0.06
Mn	1.15
Nb	0.1
Al	0.05
S	0.025
P	0.01
Si	0.02
Cu, Ni, Mo	trace
Fe	balance

Mechanical Properties	σ_y (MPa)	$\sigma_{\mu TS}$ (MPa)	n
monotonic	585	775	0.1
cyclic (') (from ref. 32)	459	---	0.25

TABLE III

Comparison of Effective Particle Sizes (D_{eff}) and Root-Mean Square Strains (ϵ^2), Averaged over $L = 50$Å.

	Program for Large Computer		On Line Fourier Analysis Minicomputer Program			
			Multi Peak Method		Single Peak Method	
	$\langle D_{eff} \rangle$ (Å)	$\langle \epsilon^2_{50} \rangle^{\frac{1}{2}} \times 10^2$	$\langle D_{eff} \rangle$ (Å)	$\langle \epsilon^2_{50} \rangle^{\frac{1}{2}} \times 10^2$	$\langle D_{eff} \rangle$ (Å)	$\langle \epsilon^2_{50} \rangle^{\frac{1}{2}} \times 10^2$
Filed iron powder (a)	270	—	279±11	0.192	280±19	0.155
Filed β brass powder (a)	145	0.316	142±12	0.338	179±8	0.298
Steel (b)	195	0.27	169±2	0.264	184±21	0.301
435 Kbar shock loaded copper (c)	500	0.195	—	—	539±8	0.204

(a) Rothman, R. L. (private communication)
(b) Evans, W. P. (private communication)
(c) DeAngelis, R. J. (private communication)

TABLE IV

Effective Particle Size and Root-Mean-Square Strain as a Function of Uniaxial Plastic Deformation.

Cumulative Strain (%)*	Effective Particle Size (Å)	Root mean square Strain, $\langle \epsilon_{50}^{2} \rangle^{\frac{1}{2}} \times 10^{2}$
0.0	> 3500	-----
1.0	1280	0.08
2.0	1050	0.10
3.0	1310	0.09
4.0	1070	0.11
> 15.0 (necking)	490	0.24

(*) Cumulative elongation measured from the onset of yielding divided by the initial gage length.

TABLE V

Comparison Of Measured Plastic Zone Sizes With Those Calculated From Theoretical Models.

		ANGLE RELATIVE TO CRACK PLANE, θ (°)	$\alpha(\theta) = r(\theta)/(K_I/\sigma_y)^2$	r(θ) (μm)
Measured	Statically loaded sample*(using K_I)	0	0.19	500
		90	0.30	800
	Fatigued sample (using ΔK_I)	0	0.25	700
		90	0.18	500
	Fatigued sample (using $K_{I\,max}$)	0	0.23	700
		90	0.16	500
Theory	Work hardening plane stress	0	0.33	930
		90	0.21	600
	Work hardening plane strain	0	0.00	0
		90	0.24	680

(*) $(K_I/\sigma_y)^2$ = 2.82 mm used for calculated values.

FIGURE CAPTIONS

Fig. 1 Plastic zone boundary for a work hardening material subjected to mode I loading. Poisson's ratio = 0.3. Zone for plane strain calculated from ref. 1, that for plane stress from ref. 2, 3.

Fig. 2

Nominal dimensions (in millimeters) for all types of specimens.

	SAMPLE TYPE	OVERALL LENGTH	OVERALL WIDTH	OVERALL THICKNESS	GAUGE LENGTH	GAUGE WIDTH
		(mm.)				
2a	Tensile monotonic stress-strain(a)	152.4	25.4	2.8	89.0	12.7
2a	Tensile x-ray elastic constant determination(a)	127.0	25.4	1.8	89.0	10.2
2a	Tensile plastic deformation comparison (a)	127.0	25.4	1.0	89.0	6.3
2b	High cycle fatigue (b)	127.0	25.4	2.0	---- crack length 5.6	----

Fig. 3 Static load applied, sample with notch. $\sigma/\sigma_y = 0.52$, $K_I = 30.2$ MPa$\cdot m^{\frac{1}{2}}$. Plastic zone shown shaded (where $D_{eff} > 2500\text{Å}$): a) longitudinal stress σ_{yy}, b) transverse stress σ_{xx}.

Fig. 4 Longitudinal stress, σ_{yy}, measured after static load removed for sample with notch $\sigma/\sigma_y = 0.52$, $K_I = 30.2$ MPa$\cdot m^{\frac{1}{2}}$. Plastic zone shown shaded.

Fig. 5 After etching one quarter of the way to the center of sample with notch, load removed. $\sigma/\sigma_y = 0.52$, $K_I = 30.2$ MPa$\cdot m^{\frac{1}{2}}$. Plastic zone shown shaded. a) σ_{yy}, b) σ_{xx}.

Fig. 6 After 70,000 cycles in pull-pull fatigue, load removed. $\Delta\sigma/\sigma_y' = 0.45$, $\Delta K_I = 31.3$ MPa$\cdot m^{\frac{1}{2}}$. Plastic zone shown shaded. a) σ_{yy}, b) σ_{xx}.

Fig. 7 Dislocation density (X $10^{-13} m^{-2}$) for sample with notch, static load applied. $\sigma/\sigma_y = 0.52$, $K_I = 30.2$ MPa$\cdot m^{\frac{1}{2}}$. Plastic zone shown shaded.

Fig. 8 Dislocation density (X $10^{-13} m^{-2}$) for sample with notch static load removed. $\sigma/\sigma_y = 0.52$, $K_I = 30.2$ MPa$\cdot m^{\frac{1}{2}}$. Plastic zone shown shaded.

Fig. 9 Dislocation density (X $10^{-13} m^{-2}$) for sample with fatigue crack after 70,000 cycles in pull-pull fatigue, load removed. $\Delta\sigma/\sigma_y' = 0.45$, $\Delta K_I = 31.3$ MPa$\cdot m^{\frac{1}{2}}$. Plastic zone shown shaded.

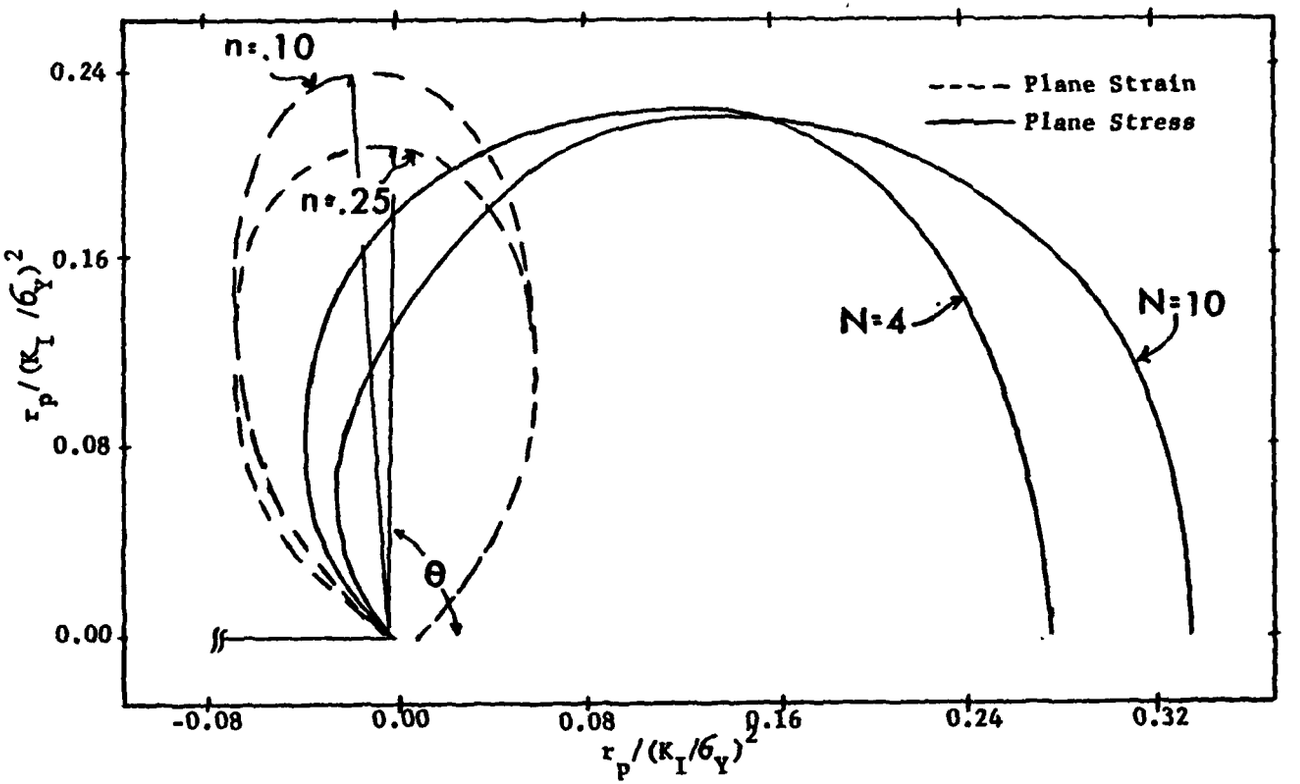

FIGURE 1

W. H. Schlosberg and J. B. Cohen

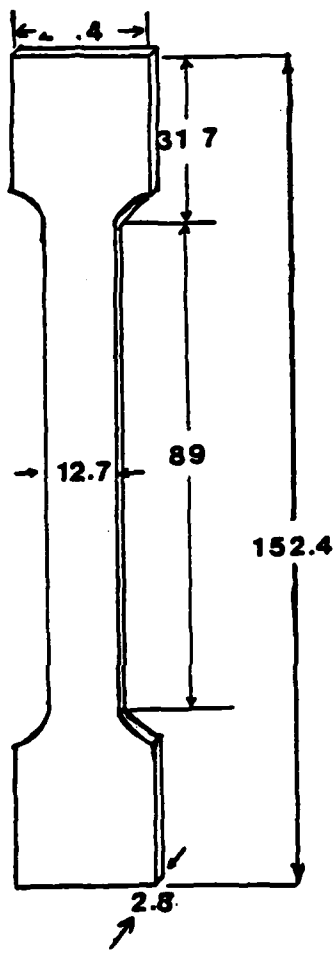

FIGURE 2a

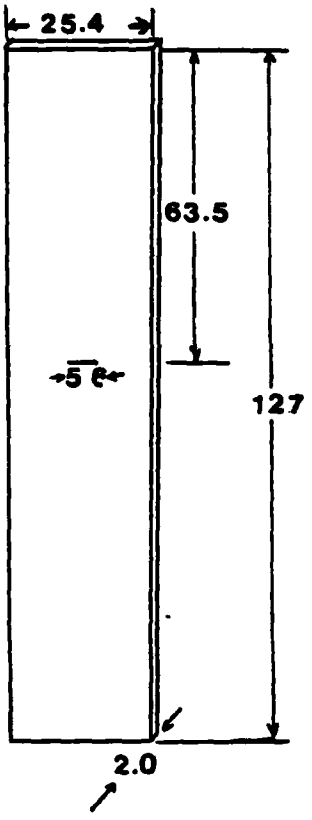

FIGURE 2b

W. H. Schlosberg and J. B. Cohen

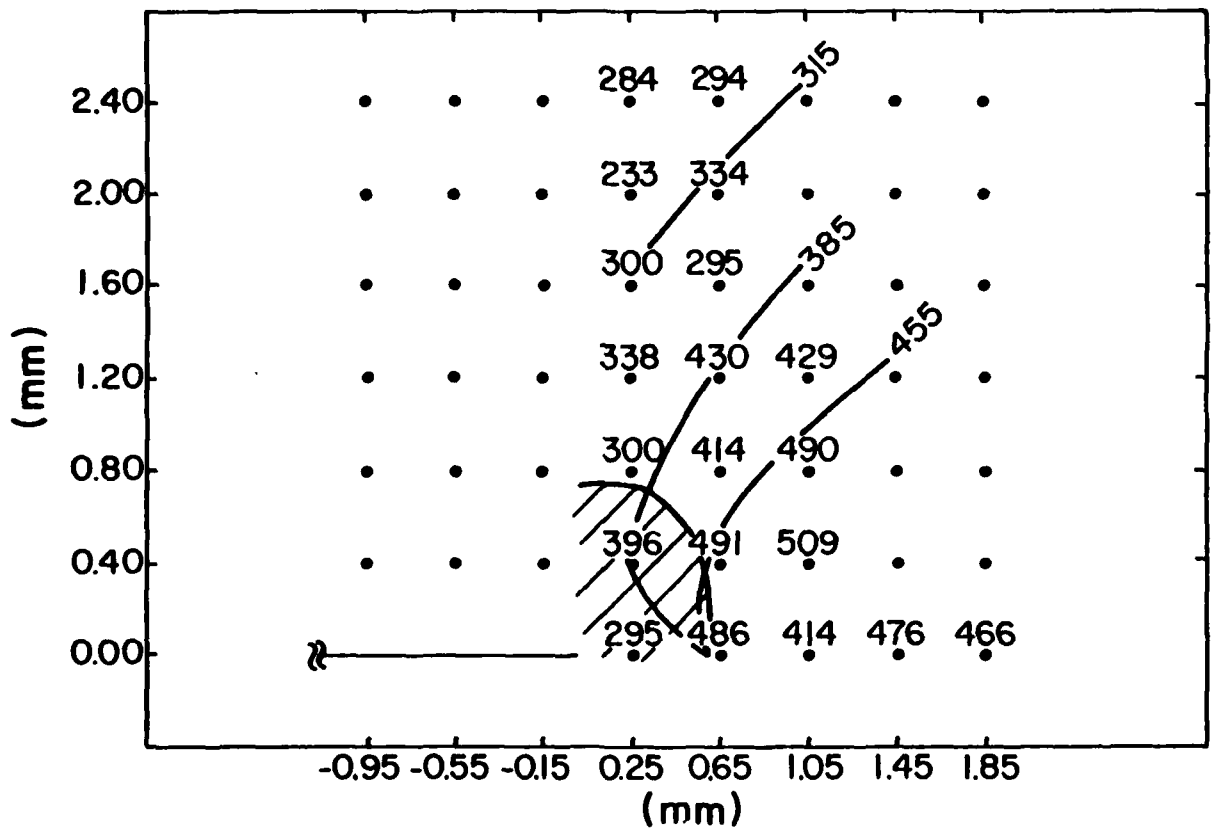

FIGURE 3a

W. H. Schlosberg and J. B. Cohen

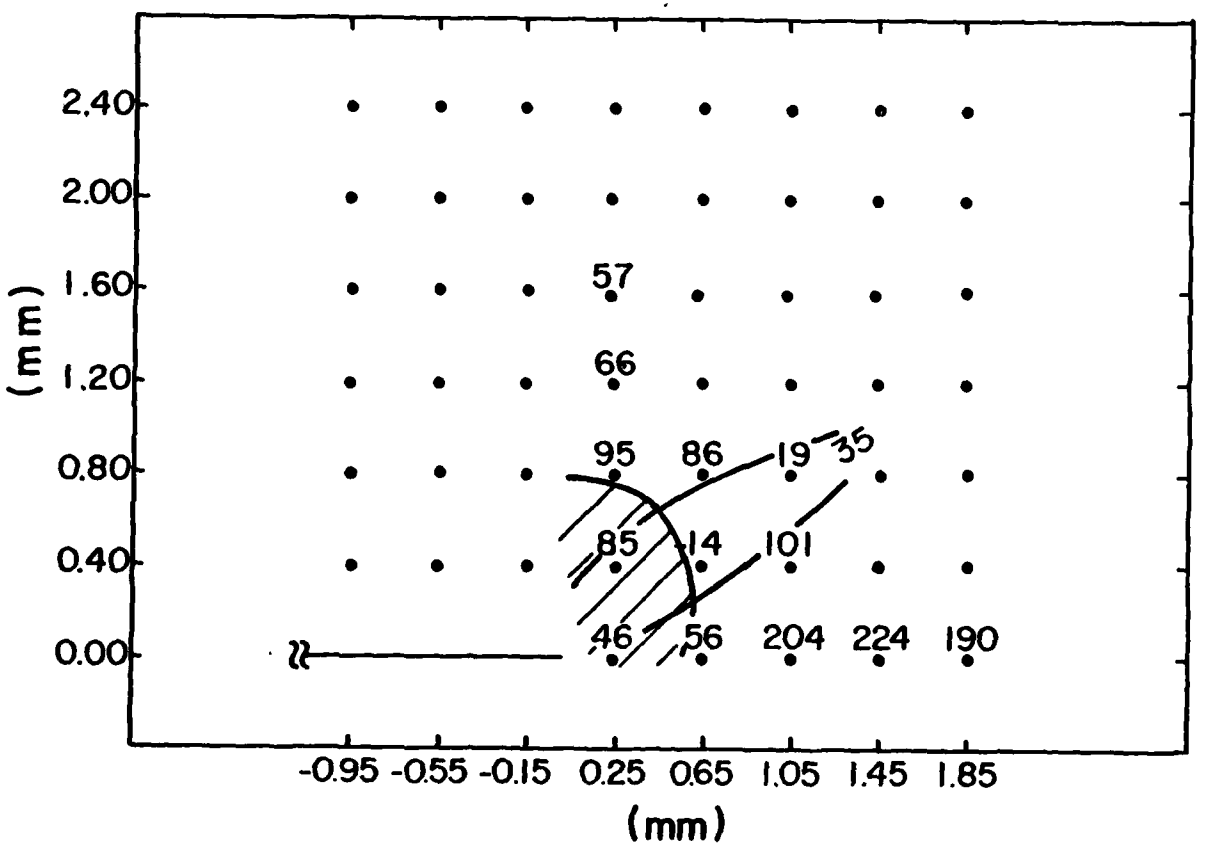

FIGURE 3b

W. H. Schlosberg and J. B. Cohen

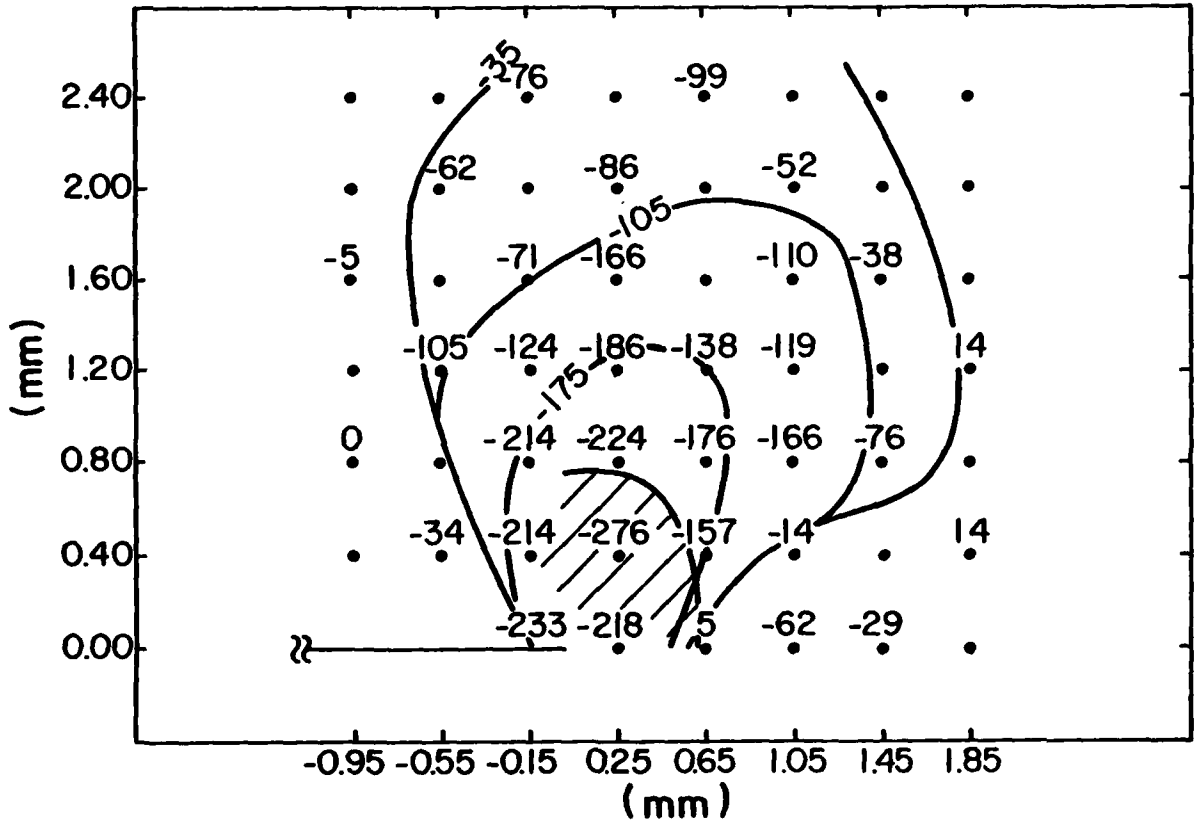

FIGURE 4

W. H. Schlosberg and J. B. Cohen

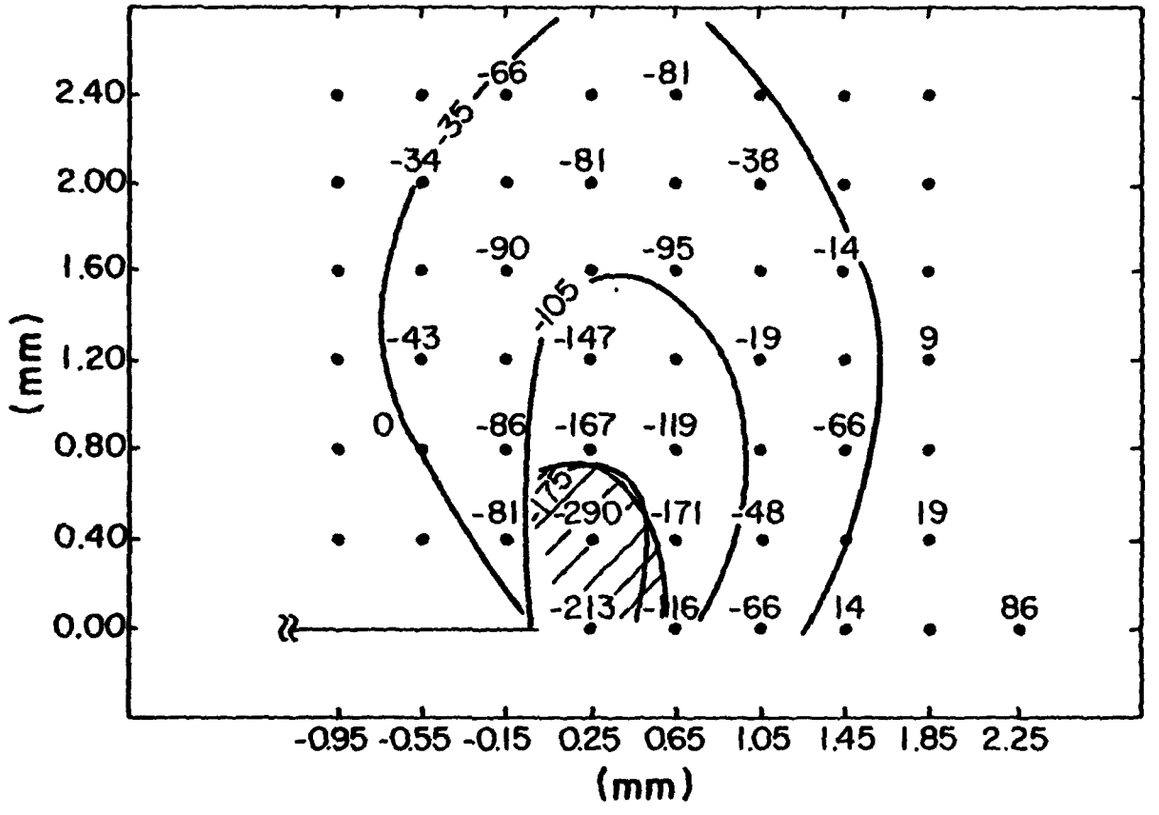

FIGURE 5a

W. H. Schlosberg and J. B. Cohen

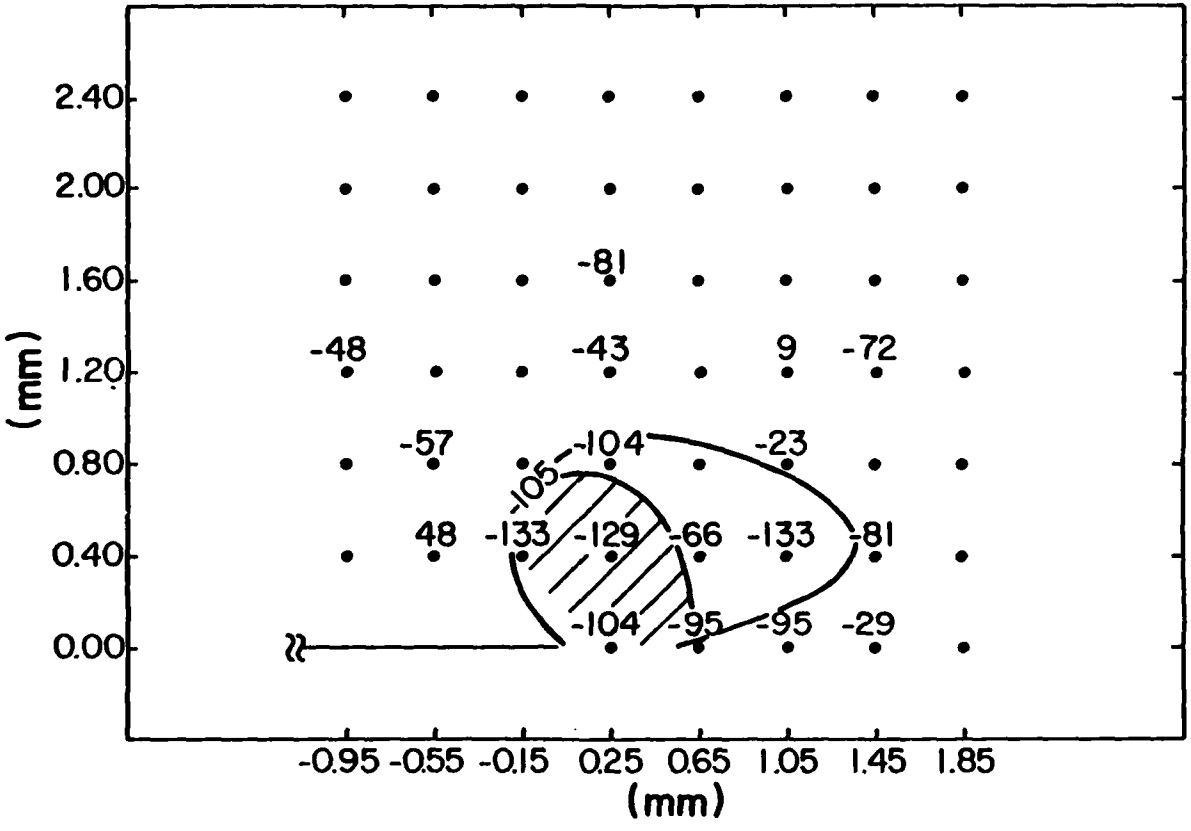

FIGURE 5b

W. H. Schlosberg and J. B. Cohen

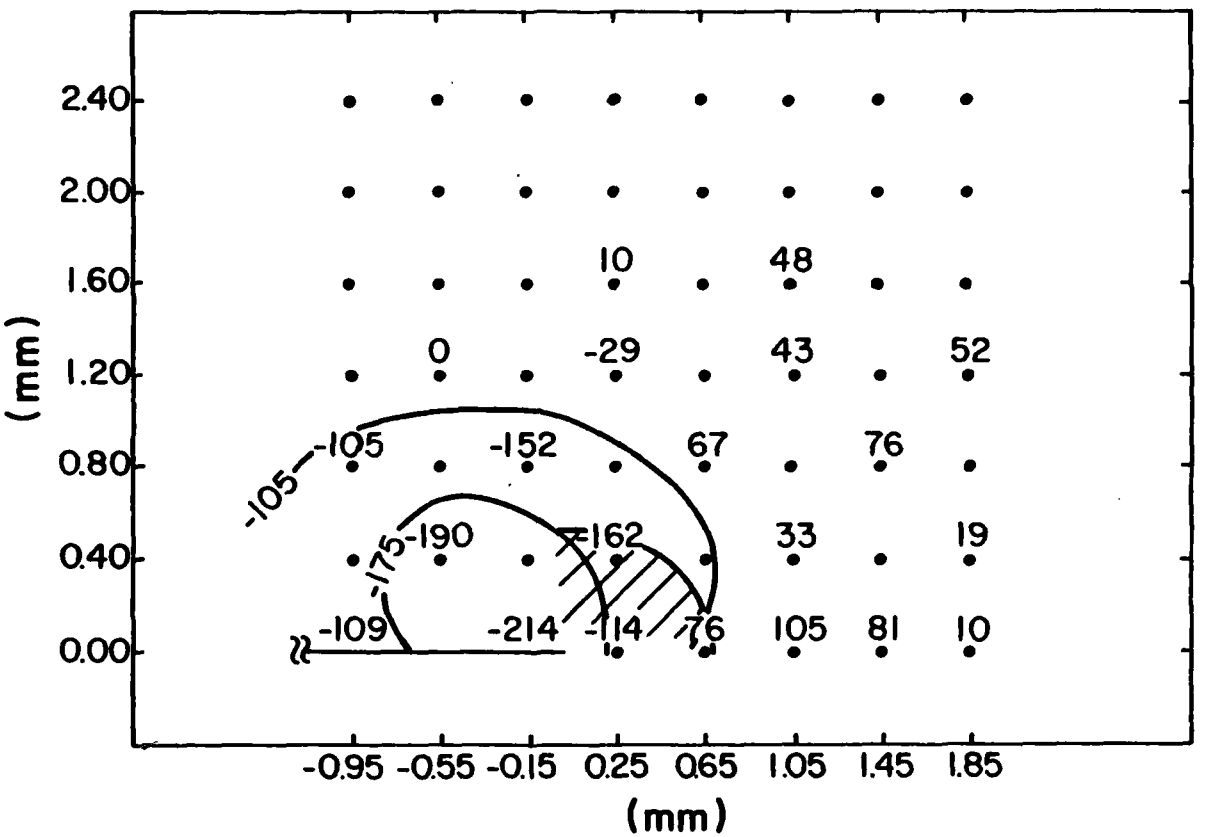

FIGURE 6a

W. H. Schlosberg and J. B. Cohen

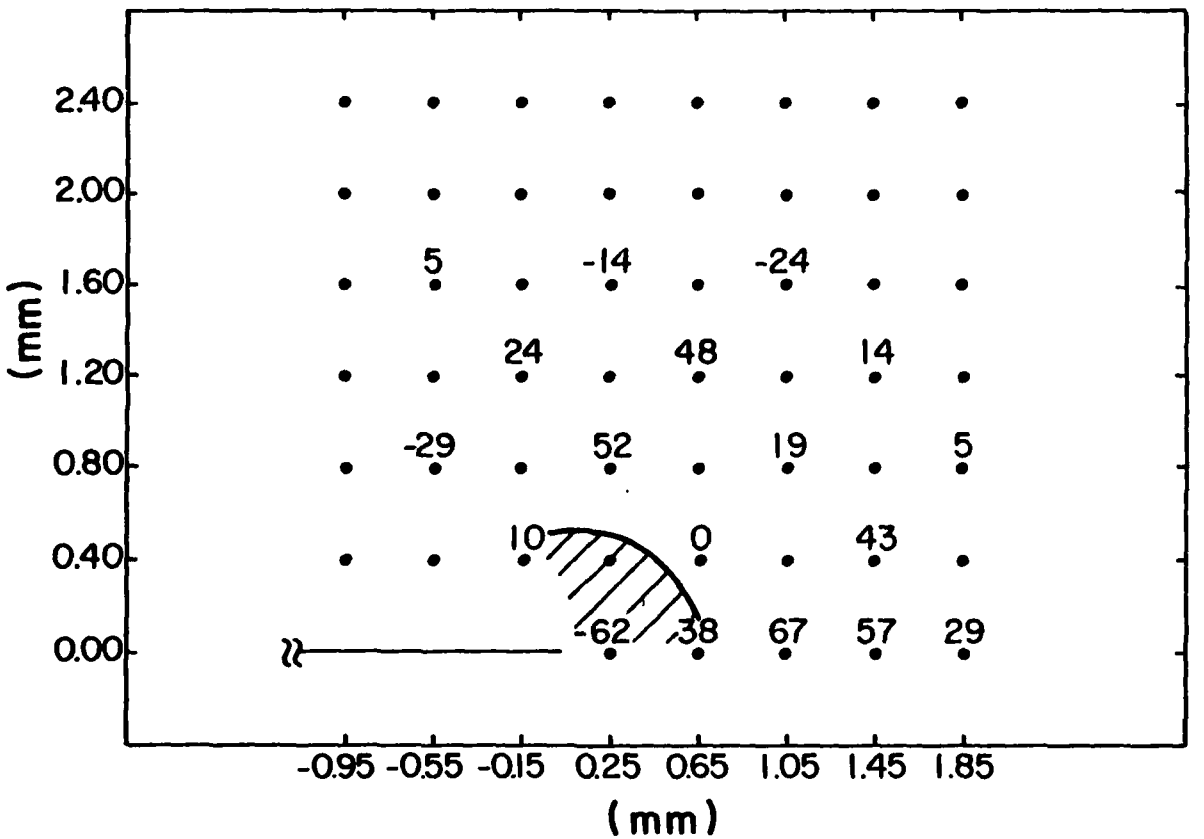

FIGURE 6b

W. H. Schlosberg and J. B. Cohen

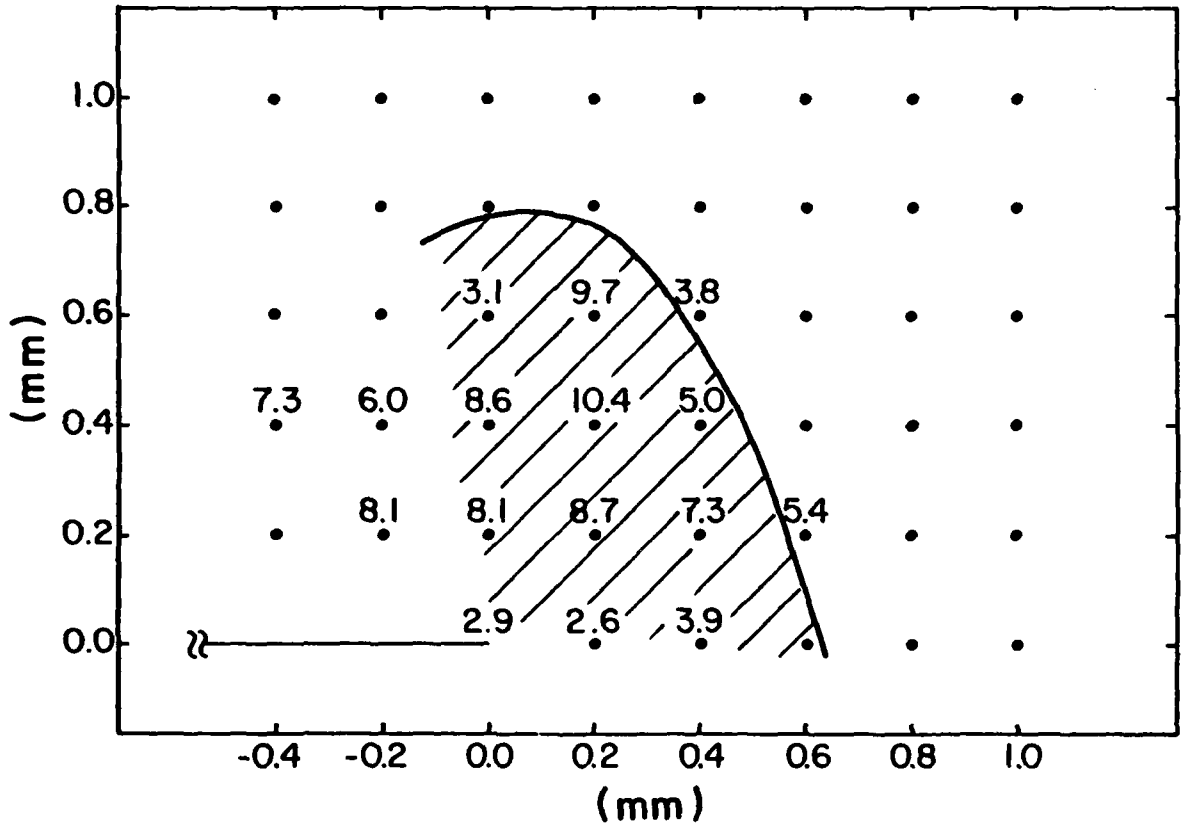

FIGURE 7

W. H. Schlosberg and J. B. Cohen

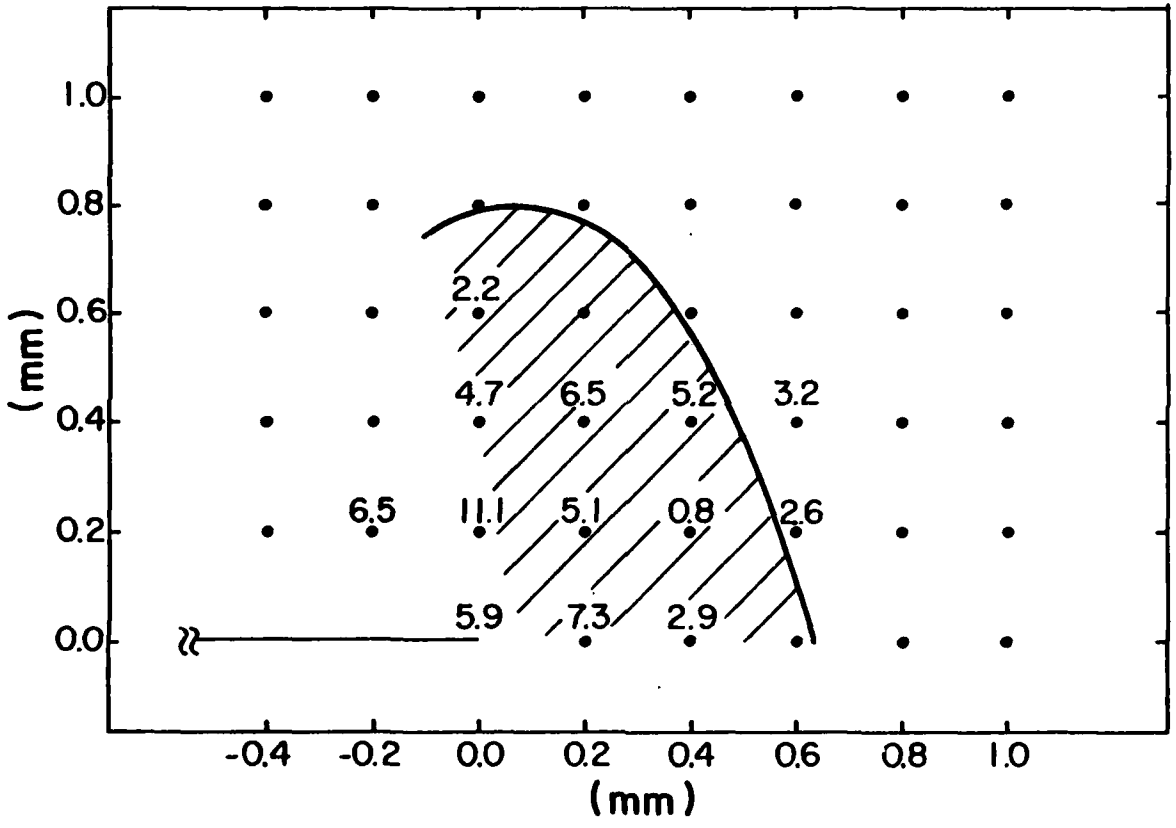

FIGURE 8

W. H. Schlosberg and J. B. Cohen

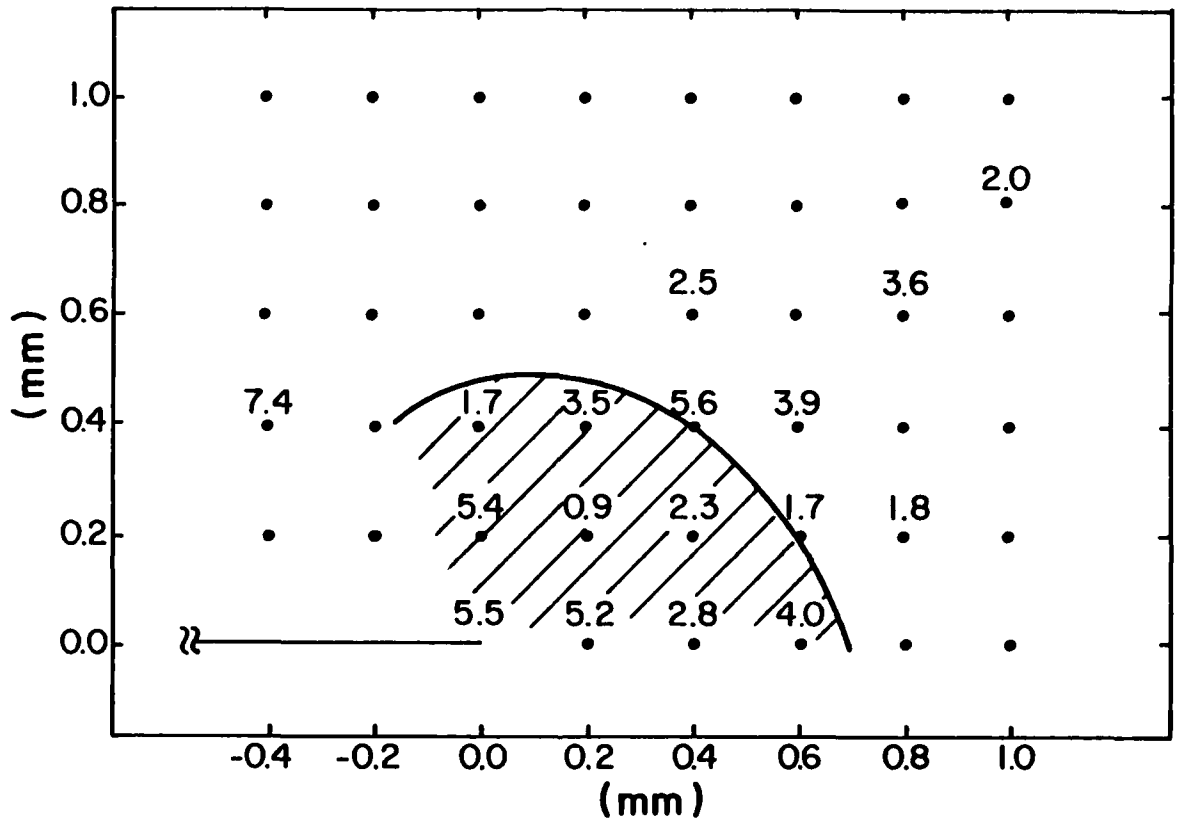

FIGURE 9

W. H. Schlosberg and J. B. Cohen

Security Classification

DOCUMENT CONTROL DATA - R & D

Security classification of title, body of abstract and indexing annotation must be entered when the overall report is classified)

1. ORIGINATING ACTIVITY (Corporate author)	2a. REPORT SECURITY CLASSIFICATION
J. B. Cohen Northwestern University Evanston, Illinois 60201	Unclassified 2b. GROUP

3. REPORT TITLE

THE PLASTIC ZONE AND RESIDUAL STRESS NEAR A NOTCH AND A FATIGUE CRACK IN HSLA STEEL

4. DESCRIPTIVE NOTES *(Type of report and inclusive dates)*

Technical Report No. 5

5. AUTHOR(S) *(First name, middle initial, last name)*

W. H. Schlosberg and J. B. Cohen

6. REPORT DATE	7a. TOTAL NO. OF PAGES	7b. NO. OF REFS
December 16, 1981	55	55

8a. CONTRACT OR GRANT NO	9a. ORIGINATOR'S REPORT NUMBER(S)
N00014-80-C-0116	
b. PROJECT NO Mod. No. P00002	5
c.	9b. OTHER REPORT NO(S) *(Any other numbers that may be assigned this report)*
d.	

10. DISTRIBUTION STATEMENT

Distribution of this document is unlimited

11. SUPPLEMENTARY NOTES	12. SPONSORING MILITARY ACTIVITY
	Metallurgy Branch Office of Naval Research

13. ABSTRACT

The plastic zone and residual stress around a notch under load and with the load removed, and around a fatigue crack (at the same stress intensity factor as for the notch) have been examined, with automated X-ray techniques and a microbeam. There is good agreement between the measured plastic zone size and Hutchinson's theory for a work hardening material. Residual stresses exist well behind the tip, and vary with depth, so that measurements of crack closure on a surface may not be directly related to closure stress (which samples the bulk). Instabilities in the dislocation arrangement can be detected by comparing X-ray line broadening of bulk specimens under load, and with the load removed.

14 KEY WORDS	LINK A		LINK B		LINK C	
	ROLE	WT	ROLE	WT	ROLE	WT
stresses, residual stresses, fatigue, plastic zone closure.						